J|A|C|S
ARTICLES
Published on Web 06/28/2003

Mechanistic Implications for the Formation of the Diiron Cluster in Ribonucleotide Reductase Provided by Quantitative EPR Spectroscopy

Brad S. Pierce,[†] Timothy E. Elgren,[‡] and Michael P. Hendrich*[,†]

Contribution from the Department of Chemistry, Carnegie Mellon University, Pittsburgh, Pennsylvania 15213, and Department of Chemistry, Hamilton College, Clinton, New York 13323

Received October 21, 2002; E-mail: hendrich@andrew.cmu.edu

Abstract: The small subunit of *Escherichia coli* ribonucleotide reductase (R2) is a homodimeric ($\beta\beta$) protein, in which each β-peptide contains a diiron cluster composed of two inequivalent iron sites. R2 is capable of reductively activating O_2 to produce a stable tyrosine radical (Y122•), which is essential for production of deoxyribonucleotides on the larger R1 subunit. In this work, the paramagnetic Mn^{II} ion is used as a spectroscopic probe to characterize the assembly of the R2 site with EPR spectroscopy. Upon titration of Mn^{II} into samples of apoR2, we have been able to quantitatively follow three species (aquaMn^{II}, mononuclear Mn^{II}R2, and dinuclear Mn_2^{II}R2) and fit each to a sequential two binding site model. As previously observed for Fe^{II} binding within apoR2, one of the sites has a greater binding affinity relative to the other, $K_1 = (5.5 \pm 1.1) \times 10^5\ M^{-1}$ and $K_2 = (3.9 \pm 0.6) \times 10^4\ M^{-1}$, which are assigned to the B and A sites, respectively. In multiple titrations, only one dinuclear Mn_2^{II}R2 site was created per homodimer of R2, indicating that only one of the two β-peptides of R2 is capable of binding Mn^{II} following addition of Mn^{II} to apoR2. Under anaerobic conditions, addition of only 2 equiv of Fe^{II} to R2 (Fe_2^{II}R2) completely prevented the formation of any bound MnR2 species. Upon reaction of this sample with O_2 in the presence of Mn^{II}, both Y122• and Mn_2^{II}R2 were produced in equal amounts. Previous stopped-flow absorption spectroscopy studies have indicated that apoR2 undergoes a protein conformational change upon binding of metal (Tong et al. *J. Am. Chem. Soc.* **1996**, *118*, 2107−2108). On the basis of these observations, we propose a model for R2 metal incorporation that invokes an allosteric interaction between the two β-peptides of R2. Upon binding the first equiv of metal to a β-peptide (β_I), the aforementioned protein conformational change prevents metal binding in the adjacent β-peptide (β_{II}) approximately 25 Å away. Furthermore, we show that metal incorporation into β_{II} occurs only during the O_2 activation chemistry of the β_I-peptide. This is the first direct evidence of an allosteric interaction between the two β-peptides of R2. Furthermore, this model can explain the generally observed low Fe occupancy of R2. We also demonstrate that metal uptake and this newly observed allosteric effect are buffer dependent. Higher levels of glycerol cause loss of the allosteric effect. Reductive cycling of samples in the presence of Mn^{II} produced a novel mixed metal $Fe^{III}Mn^{III}$R2 species within the active site of R2. The magnitude of the exchange coupling (J) determined for both the Mn_2^{II}R2 and $Fe^{III}Mn^{III}$R2 species was determined to be -1.8 ± 0.3 and $-18 \pm 3\ cm^{-1}$, respectively. Quantitative spectral simulations for the $Fe^{III}Mn^{III}$R2 and mononuclear Mn^{II}R2 species are provided. This work represents the first instance where both X- and Q-band simulations of perpendicular and parallel mode spectra were used to quantitatively predict the concentration of a protein bound mononuclear Mn^{II} species.

Ribonucleotide reductase (RNR)[1] catalyzes the reduction of ribonucleotides to deoxyribonucleotides necessary for DNA synthesis.[2] As isolated from *Escherichia coli*, RNR is composed of two nonidentical homodimeric subunits ($\alpha_2\beta_2$). The α_2 subunit (R1) is the larger of the two homodimers and contains the substrate binding site and two allosteric sites. The active site of the R1 subunit is composed of 5 redox-active dithiols derived from cysteines.[2,3] These cysteines are ultimately responsible for the reduction of the ribonucleotide within the R1 active site.[4]

Each polypeptide within the smaller β_2 subunit (R2) contains a binuclear non-heme iron site. This subunit belongs to a diverse group of proteins that are capable of reductively activating O_2 to perform a variety of biological reactions.[5] In the reduced state ($R2_{red}$), the diferrous site can reductively activate O_2 and,

[†] Department of Chemistry, Carnegie Mellon University.
[‡] Department of Chemistry, Hamilton College.
(1) See Abbreviations paragraph at the end of the paper.
(2) Stubbe, J. *J. Adv. Enzymol. Related Areas Mol. Biol.* **1989**, *63*, 349−419.
(3) Reichard, P. *TIBS* **1997**, *22*, 81−85.
(4) Stubbe, J. *J. Biol Chem.* **1990**, 265, *10*, 5329−5333.
(5) Feig, A.; Lippard, S. J. *Chem Rev.* **1994**, *94*, 759−805.

10.1021/ja021290h CCC: $25.00

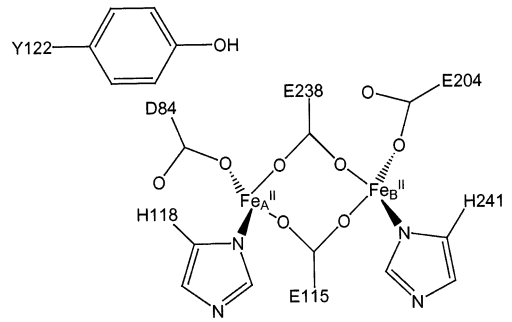

Figure 1. Schematic representation of the diferrous R2 active site adapted from refs 7, 17.

combined with an "extra" electron, produce a stable tyrosine radical (Y122•) adjacent to the diiron active site. The radical is essential for the catalytic activity of RNR.[5−18] The structure of the diferrous clusters in $R2_{red}$ is shown in Figure 1,[7,17,18] and the radical generating reaction is shown below

$$3Fe^{II} + Y122\text{-}OH + O_2 + H^+ \rightarrow Fe^{III}(O^{2-})Fe^{III} + Y122\text{-}O\bullet + Fe^{III} + H_2O$$

The complete reduction of O_2 to H_2O by $R2_{red}$ requires four electrons, three of which are derived from the diiron cluster and Y122. In the absence of an additional reductant, Fe^{II} can serve as the source of this "extra" electron. Thus, resulting in the 3:1 Fe^{II} to Y122• stoichiometry generally observed.[13,19−22] Although the above reaction implies that each β-peptide of R2 is capable of generating Y122•, on average only 1.2 Y122• per R2 are observed. Furthermore, preparations of R2 from multiple laboratories typically observe only 3.2 to 3.4 Fe atoms per R2.[15,22,23,28,32] The reason R2 exhibits less than the theoretical limit of Y122• and Fe incorporation is not well understood.

While in its active state ($R2_{act}$), formally [$Fe^{III}(O^{2-})Fe^{III}$; Y122•], the tyrosine radical is believed to participate in a long-range electron transfer (∼35 Å) to form a cysteinyl radical in the R1 subunit active site.[4,15,24] During the O_2 activation of R2, a high-valent intermediate termed **X**, formally [$(H_2O)Fe^{III}$-$(O^{2-})Fe^{IV}$], has been shown to be a precursor to the generation of a tyrosine radical at Tyr122.[25−27]

Previous studies have demonstrated that although formation of **X** is independent of Fe^{II} and O_2 concentration, formation of **X** is first-order in apoR2. Therefore, neither Fe^{II} nor O_2 can be involved in the rate-limiting step. Additionally, preloading apoR2 with 2 equivalents of Fe^{II} prior to introduction of O_2 increases the rate of **X** formation by an order of magnitude (8 s^{-1} vs 60−80 s^{-1}).[21,28] Therefore, it was proposed that initial binding of the first Fe^{II} is followed by a protein conformational change prior to binding the second Fe^{II}.[29,30] Moreover, it has been reported that during the assembly of the diferrous active site, shown in Figure 1, the two iron binding sites within a R2 monomer have different binding affinities. Mössbauer and MCD studies have shown that the Fe_B site[31] (or Fe2, 8.3 Å from Y122) exhibits approximately a 5-fold greater binding affinity for Fe^{II} than the Fe_A site (or Fe1, 5.3 Å from Y122).[17,18,32,33] The current model for assembly of the diferrous site of R2 involves noncooperative binding of Fe^{II} by both β-peptides independently of each other; sequentially occupying the Fe_B site of each β-peptide prior to the Fe_A sites.[21,32,33]

Protein-bound Fe^{II} is spectroscopically difficult to differentiate from free Fe^{II} in solution and to quantify accurately in low concentrations. This and the high oxygen sensitivity of $R2_{red}$ make characterization of the active site assembly experimentally difficult. For these reasons, Mn is an attractive spectroscopic probe for metal incorporation into R2. Manganese(II) has been shown to bind tightly within the active site of R2 with the same ligation as Fe^{II}.[32,34,35] The Mn^{II} binding affinity must be comparable to Fe^{II} because addition of Fe^{II} to Mn^{II} incorporated R2 does not displace detectable amounts of Mn^{II}.[34] In addition, Mn^{II} can serve as a probe for studying the assembly of the initial $Fe_2^{II}R2$ complex without the complication of further oxygen chemistry taking place. Finally, the various species of Mn^{II} are readily identifiable and quantified with EPR spectroscopy.

In the present study, Mn^{II} is used to probe the metal binding properties of R2. The formation of three spectroscopically distinct paramagnetic species were quantitatively monitored with EPR spectroscopy: mononuclear $Mn^{II}R2$, dinuclear $Mn_2^{II}R2$, and aquaMn^{II}. The results will show that only 2 Mn^{II} ions are taken up sequentially (noncooperative binding) within a single

(6) Wallar, B. J.; Lipscomb, J. D. *Chem Rev.* **1996**, *96*, 2625−2657.
(7) Nordlund, P.; Eklund, H. *J. Mol. Biol.* **1993**, *232*, 123−164.
(8) Bollinger, J. M., Jr; Krebs, C.; Vicol, A.; Chen, S.; Ley, B. A.; Edmondson, D. E.; Huynh, B. H. *J. Am. Chem. Soc.* **1998**, *120*, 1094−1095.
(9) Nordlund, P.; Åberg, A.; Uhlin, U.; Eklund, H. *Biochem. Soc. Trans.* **1993**, *21*, 735−738.
(10) Nordlund, P., Sjöberg, B. M.; Eklund, H. *Nature* **1990**, *345*, 593−598.
(11) Thelander, L. *J. Biol. Chem.* **1974**, *249*, No. 15, 4858-4862.
(12) Reichard, P. *Science* **1993**, *260*, 1773−1777.
(13) Bollinger, J. M., Jr; Edmondson, D. E., Huynh, B. H., Filley, J., Norton, J. R.; Stubbe, J *Science* **1991**, *253*, 292−298.
(14) Baldwin, J.; Krebs, C.; Ley, B. A.; Edmondson, D. E.; Huynh, B. H.; Bollinger, J. M., Jr.; *J. Am. Chem. Soc.* **2000**, *122*, 12195−12206.
(15) Lynch, J. B.; Juarez-Garcia, C.; Münck, E.; Que, L., Jr. *J. Biol. Chem.* **1989**, *264*, 14, 8091−8096.
(16) Atkin, C. L.; Thelander, L.; Reichard, P.; Lang, G. *J. Biol. Chem.* **1973**, *248*, 7464−7472.
(17) Logan, D. T.; Su, X.-D.; Åberg, A.; Regnström, K.; Hajdu, J.; Eklund, H.; Nordlund, P. *Structure* **1996**, *4*, 9, 1054−1064.
(18) Andersson, M. E.; Högbom, M.; Rinaldo-Matthis, A.; Andersson, K. K.; Sjöberg, B. M.; Nordlund, P. *J. Am. Chem. Soc.* **1999**, *121*, 2346−2352.
(19) Elgren, T. E.; Lynch, J. B.; Juarez-Garcia, C.; Münck, E, Sjöberg, B.-M.; Que, L., Jr. *J. Biol. Chem.* **1991**, *266*, 19 265−19 268.
(20) Bollinger, M. J., Jr. Ph.D. Thesis, Massachusetts Institute of Technology, 1993.
(21) Bollinger, J. M., Jr.; Tong, W. H.; Ravi, N.; Huynh, B. H.; Edmondson, D. E.; Stubbe, *J. Am. Chem. Soc.* **1994**, *116*, 8015−8023.
(22) Ochiai, E. I.; Mann, G. J.; Gräslund, A.; Thelander, L. *J. Biol. Chem.* **1990**, *265*, 26, 15 758−15 761.
(23) Sjöberg, B.-M.; Karlsson, M.; Jörnvall, H. *J. Biol. Chem.* **1987**, *262*, 20, 9736−9743.
(24) Silva, K. E.; Elgren, T. E.; Que, L. Jr.; Stankovich, M. T. *Biochemistry* **1995**, *34*, 14 093−14 103.
(25) Sturgeon, B. E.; Burdi, D.; Chen, S.; Huynh, B. H.; Edmondson, D. E.; Stubbe, J.; Hoffman, B. M. *J. Am. Chem. Soc.* **1996**, *118*, 7551−7557.
(26) Willems, J.-P.; Lee, H.-I.; Burdi, D.; Doan, P. E.; Stubbe, J.; Hoffman, B. M. *J. Am. Chem. Soc.* **1997**, *119*, 9816−9824.
(27) Burdi, D.; Willems, J.-P.; Riggs-Gelasco, P. Antholine, W. E.; Stubbe, J.; Hoffman, B. M. *J. Am. Soc. Chem.* **1998**, *120*, 12 910−12 919.
(28) Ravi, N.; Bollinger, J. M., Jr.; Huynh, B. H.; Edmondson, D. E.; Stubbe, J. *J. Am. Chem. Soc.* **1994**, *116*, 8007−8014.
(29) Tong, W. H.; Chen, S.; Lloyd, S. G.; Edmondson, D. E.; Huynh, B. H.; Stubbe, J. *J. Am. Chem. Soc.* **1996**, *118*, 2107−2108.
(30) Umback, N. J.; Norton, J. R. *Biochemistry* **2002**, *41*, 3984−3990.
(31) The use of Fe_A and Fe_B to designate the crystallographic iron sites Fe1 and Fe2 reported by Norlund et al. was originally invoked by Ravi et al. (ref 28) to clarify comparisons made between the crystallographic work and their Mössbauer assignments. Subsequently, this nomenclature has been adopted by several other researchers spectroscopically characterizing the individual iron binding sites of R2.
(32) Yang, Y. S.; Baldwin, J.; Ley, B. A.; Bollinger, M. J., Jr.; Solomon, E. I. *J. Am. Chem. Soc.* **2000**, *122*, 8495−8510.
(33) Bollinger, M. J., Jr.; Chen, S.; Parkin, S. E.; Mangravite, L. M.; Ley, B. A.; Edmondson, D. E.; Huynh, B. H. *J. Am. Chem. Soc.* **1997**, *119*, 5976−5977.
(34) Atta, M.; Nordlund, P.; Åberg, A.; Eklund, H.; Fontecave, M. *J. Biol Chem.* **1992**, *267*, 29, 20 682−20 688.
(35) Stemmler, T. L.; Sossong, T. M.; Goldstein, J. I.; Ash, D. E.; Elgren, T. E.; Kurtz, D. M.; Penner-Hahn, J. E. *Biochemistry* **1997**, *36*, 9847−9858.

β-peptide of the R2 homodimer ($\beta\beta$). This indicates that the two β-peptides of R2 do not act independently during metal incorporation. Therefore, we introduce nomenclature to differentiate the β-peptide forming a bimetallic cluster first as β_I and the adjacent second β-peptide as β_{II}. The two β-peptides of R2 exhibit negative homotropic allosteric interaction during metal binding at the active sites. Incorporation of Mn^{II} into the β_{II}-peptide only occurs during or after the activation of R2 with O_2. We will propose this turnover-dependent metal binding explains the low Fe occupation of the protein that is generally observed.[15,22,23,28,32]

Quantitative X-band (perpendicular and parallel mode) and Q-band (perpendicular mode) simulations are provided for the mononuclear Mn^{II}R2 species, which is novel for Mn^{II} sites with larger zero-field splitting. Reductive cycling samples of Fe_2^{II}-R2 in the presence of Mn^{II} produced an additional minority species, which could be assigned to a new antiferromagnetically coupled $Fe^{III}Mn^{III}$R2 center and quantitatively simulated. Furthermore, because this signal can be reductively quenched only in the presence of the mediator methyl viologen, we conclude that it must originate from a cluster within the protein and not adventitiously bound.

Materials and Methods

Protein Purification. R2 was isolated from an overproducing strain of *E coli* N6405/pSPS2 as previously described.[21,36,37] During purification proteolytic degradation of R2 was decreased by addition of a general purpose cocktail of protease inhibitors (Sigma P 2714). The integrity of R2 β-peptides was confirmed by a previously outlined anion exchange FPLC technique.[23,38] Samples were eluted on a POROS HQ/H 4.6 mmD/100 mmL FPLC column (PerSeptive Biosystems) by NaCl gradient (0−700mM) in 25mM Hepes, pH 7.6. Peak detection was performed spectrophotometrically at 280 nm. The apoR2 was prepared as previously described.[16,20,37] After iron chelation, the buffer was exchanged by passing the protein solution down a Sephadex G-25 size exclusion column [1.9 × 38 cm] equilibrated with 25mM HEPES, 100 mM KCl, 5% glycerol, pH 7.6. Significant amounts of denatured R2 were produced during chelation. After the column, the denatured protein was pelleted with centrifugation. UV−vis measurements were made on a HP 8453 spectrophotometer equipped with a constant temperature cuvette holder. The protein concentration was determined spectrophotometrically from the absorbance at 280 nm [ϵ_{280} = 141 $mM^{-1}cm^{-1}$ (R2) and 126 $mM^{-1}cm^{-1}$ (apoR2)].[37]

Sample Preparation. Stock Mn^{II} and Fe^{II} solutions were prepared anaerobically by dissolving $MnCl_2$ or $Fe(NH_3)_2(SO_4)_2$ within degassed protein buffer or double distilled water, respectively. The concentration of the Mn^{II}-stock solution was confirmed by EPR. The Fe^{II}-stock solutions were assayed spectrophotometrically as described below. These stock solutions (typically 10 to 20 mM in metal) were prepared fresh prior to addition to apoR2. For each titration point, the appropriate amount of metal containing stock solution (typically 5−10 μL) was added anaerobically to solution of apoR2 (initially 150−200 μL of 1 mM R2) directly within the EPR tube with a 25 μL Hamilton gastight syringe. The solution was mixed with a second gastight syringe (250 μL) and by inversion for 5 min, and then the sample was frozen in liquid N_2.

Anaerobic Protocols. All anaerobic work was carried out on a gas train, in which analytical grade argon was passed through a copper catalyst (BASF) to remove trace O_2 impurities within the gas. The argon was then sparged through water to hydrate the gas.

Chemicals. All chemicals were purchased from Sigma, Fisher, or VWR and used without purification. The water was from a Millipore-Q filtration system or double distilled. All aqueous solutions prepared for protein work were made within a 25 mM HEPES, 100 mM KCl, 5% glycerol, pH 7.6 buffer except where noted.

Iron Analysis. The colorimetric determination of iron content by bathophenanthroline disulfonic acid was adapted from several published techniques.[39−41] For each assay, 100 μL of approximately 0.1 mM R2 was added to a microfuge tube. The protein solution was acid hydrolyzed by addition of 50 μL each of concentrated sulfuric acid and concentrated nitric acid. The resulting suspension was heated to 95 °C for 15 min. After heating, 50 μL of 30% hydrogen peroxide was added to the solution, and the sample was heated for an additional 15 min. This effectively bleached the brown color produced during acid hydrolysis and the end solution was transparent. After digestion of the sample, 1.0 mL of 3 M acetate buffer pH 7.5, 0.2 mL of 1% NH_2OH, and 0.2 mL of 0.3% bathophenanthroline disulfonic acid were added to the sample. The resulting solution (pH 4.5) was allowed to equilibrate overnight at ambient temperature to ensure complete reduction of all ferric iron to ferrous. Iron quantitation was performed spectrophotometrically (λ = 535 nm, ϵ = 22.1 $mM^{-1}cm^{-1}$).[41,42] Two standard solutions were prepared using ferrous ammonium sulfate and ferric chloride. Results of the colorimetric assay were independently verified by quantitative EPR analysis of acid hydrolyzed samples.

EPR Spectroscopy. X-band (9 GHz) EPR spectra were recorded on a Bruker ESP 300 spectrometer equipped with an Oxford ESR 910 cryostat for low-temperature measurements and a Bruker bimodal cavity for generation of the microwave fields parallel and transverse to the static field. Q-band (35 GHz) EPR spectra were recorded on a Bruker 200 spectrometer equipped with a locally built low-temperature microwave probe and a cryogenic system.[43] For both instruments, the microwave frequency was calibrated by a frequency counter and the magnetic field with a NMR gaussmeter. The temperature of both instruments was calibrated using devices from Lake Shore Cryonics. For X- and Q-band EPR, the modulation was 100 and 3 kHz, respectively. All experimental data were collected under nonsaturating conditions.

EPR Simulations. Analysis of the EPR spectra utilized the spin Hamiltonian

$$\mathbf{H}_s = \mathbf{D}\left[\mathbf{S}_z^2 - \frac{S(S+1)}{3}\right] + E(\mathbf{S}_x^2 - \mathbf{S}_y^2) + \beta\mathbf{B}\cdot\mathbf{g}\cdot\mathbf{S} + \mathbf{S}\cdot\mathbf{A}\cdot\mathbf{I} \quad (1)$$

where D and E describe the zero-field splitting (zfs), and **g** is the g-tensor.[44] Nuclear hyperfine interactions (***A***) are treated with second-order perturbation theory. Simulations of the EPR spectra are calculated from diagonalization of this equation with software created by the authors. The powder pattern is generated for a uniform spherical distribution of the magnetic field vector **B**. The transition intensities are calculated from the square of the transition moment. The spectral line width is dominated by D-strain and simulations use distributions of the D and E/D to give the correct line width, specified as σ_D and $\sigma_{E/D}$. Least squares and deconvolution analysis of the spectra are combined to allow relevant parameters to vary, while maintaining a sum of multiple species which best fits the experimental data. The simulations are generated with consideration of all intensity factors both theoretical and experimental to allow concentration determination of species.[45] This allows direct comparison of simulated spectra to the absolute intensity scale of the experimental spectrum having a known

(36) Salowe, S.; Stubbe, J. *J. Bacteriol* **1986**, *165*, 363−366.
(37) Lynch, J. B. Ph.D. Thesis, University of Minnesota, **1989**.
(38) Larsson, A.; Karlsson, M.; Sahlin, M.; Sjöberg, B.-M. *J. Biol. Chem.* **1988**, *263*, 33, 17 780−17 784.
(39) Beinert, H. *Methods Enzymol.* **1978**, *54*, 435−445.
(40) Harvey, A. E.; Smart, J. A.; Amis, E. *Anal. Chem.***1955**, *27*, 1, 26−29.
(41) Anderson, G. L.; Howard, J. B. *Biochemistry* **1984**, *23*, 2118−2122.
(42) Sandell, E. B.; Onishi, H. *Photometric Determination of Traces of Metals*, 4th ed.; Chemical Analysis, Vol. 3, Part I **1978**, 365−366.
(43) Petasis, D.; Hendrich, M. P. *J. Magn. Reson.* **1999**, *136*, 200−206.
(44) Abragam, A.; Bleaney, B. *Electronic Paramagnetic Resonance of Transition Ions*; Clarendon Press: Oxford, London, 1970.

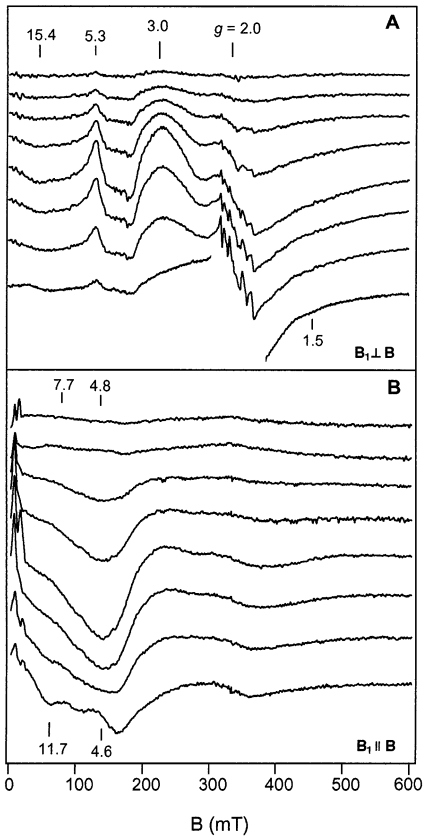

Figure 2. Representative perpendicular (A) and parallel mode (B) X-band EPR spectra showing the titration of apoR2 with Mn^{II}. The ratios of Mn^{II} added per R2 for both modes are 0.06 (top), 0.12, 0.23, 0.47, 0.82, 1.17, 1.40, and 1.75 (bottom). Instrumental conditions: temperature, 11 K; frequency, 9.62 GHz; ($B_1 \perp B$), 9.26 GHz ($B_1 \parallel B$); microwave power, 0.2 mW.

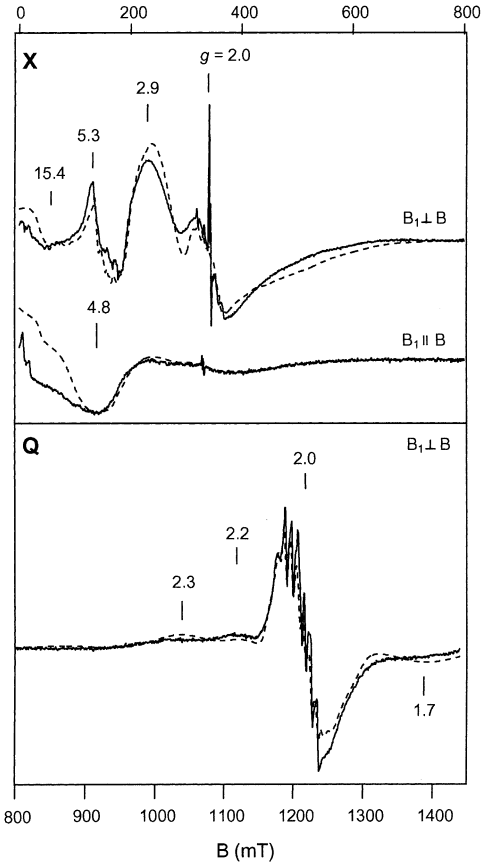

Figure 3. Perpendicular and parallel mode X-and Q-band EPR signals (solid line) and simulations (dashed line) of mononuclear $Mn^{II}R2$. Instrumental conditions: temperature, 11 K (X) 7.3 K (Q); microwave frequency, 9.62 GHz X, ($B_1 \perp B$), 9.26 GHz X, ($B_1 \parallel B$), 33.95 GHz Q, ($B_1 \perp B$); microwave power, 0.2 mW (X), 0.8 μW (Q). Simulation parameters: $g_{x,y,z} = 2.00$, $A_{x,y,z} = 8.34 \times 10^{-3}$ cm^{-1} (250 MHz), $D = 0.10$ cm^{-1}, $\sigma D = 0.03$ cm^{-1}, $E/D = 0.21$, $\sigma_{E/D} = 0.05$.

sample concentration. The only unknown factor relating the spin concentration to signal intensity is an instrumental factor that depends on the microwave detection system. However, this factor is determined by the spin standard, CuEDTA, for which the copper concentration was accurately determined from plasma emission spectroscopy.

Results

Titration of apoR2 with Manganese. Using the iron analysis protocol described in the Experimental Section, preparations of apoR2 were found to contain < 0.1 equiv of iron per R2 homodimer ($\beta\beta$). Reactivation of the apoR2 by addition of excess Fe^{II} and ascorbate followed by gel filtration gave an optical spectrum similar to that published previously.[16] The concentration of tyrosine radical was 1.2 per R2 homodimer as determined from EPR spectroscopy. Iron analysis of the reactivated R2 indicated the presence of 3.5 Fe atoms per R2 homodimer. Both of these values are comparable to the best reported values to date,[15,22,23,28,32] thus, the preparations of apoR2 were essentially free of iron and viable to reactivation.

Representative X-band EPR spectra of apoR2 as a function of added Mn^{II} are shown in Figure 2 for microwave fields ($\mathbf{B_1}$) perpendicular (A) and parallel (B) to the static magnetic field ($\mathbf{B}$). As the concentration of added Mn^{II} approaches 1.0 equiv per $\beta\beta$, EPR signals from a Mn^{II} species are observed to grow in simultaneously at $g = 15.4$, 5.3, 3.0, and 2.0 ($\mathbf{B_1} \perp \mathbf{B}$) and a broad signal with a valley at $g = 4.8$ ($\mathbf{B_1} \parallel \mathbf{B}$). In addition, a sharper signal grows in from a second species at $g = 2$ with a sharp 6-line hyperfine pattern which is characteristic of aqua-Mn^{II}. AquaMn^{II} (or free Mn^{II}) refers to Mn with predominately water coordination which is not bound to interior protein sites. Above 1 equiv, the signals from the first species decrease and are virtually absent at 2 equiv of Mn^{II} added. However, the 6-line signal from aquaMn^{II} continues to increase.

Figure 3 shows X- and Q-band EPR spectra of the Mn^{II} titration at 1 equiv of Mn^{II}. Overlaid on these spectra are quantitative simulations of a $S = 5/2$ species with $I = 5/2$. The spectra from both frequencies are fit with zero-field parameters $D = 0.10$ cm^{-1} and $E/D = 0.21$. The simulations unambiguously identify the signals as originating from a mononuclear Mn^{II}-species. The large D-value is indicative of Mn binding to a protein site, and thus, we label this species $Mn^{II}R2$. As mentioned in the Method section, the fitting protocol links the signal intensity to the sample concentrations. The amount of aquaMn^{II} in this signal is less than 0.02 equiv, and the amount of $Mn^{II}R2$ determined from the simulations is within 12% of 1 equiv. Thus, nearly all added Mn^{II} is observed as the $Mn^{II}R2$ species. The X-band features at $g = 5.3$ ($\mathbf{B_1} \perp \mathbf{B}$) and $g = 4.8$ ($\mathbf{B_1} \parallel \mathbf{B}$) originate from the $\Delta m_s = \pm 2$ transitions, whereas all other signal originate from $\Delta m_s = \pm 1$ transitions. The simulations of the parallel mode signals deviate from the data

(45) Hendrich, M. P.; Petasis, D.; Arciero, D. M.; Hooper, A. B. *J. Am. Chem. Soc.* **2001**, *123*, 2997−3005.

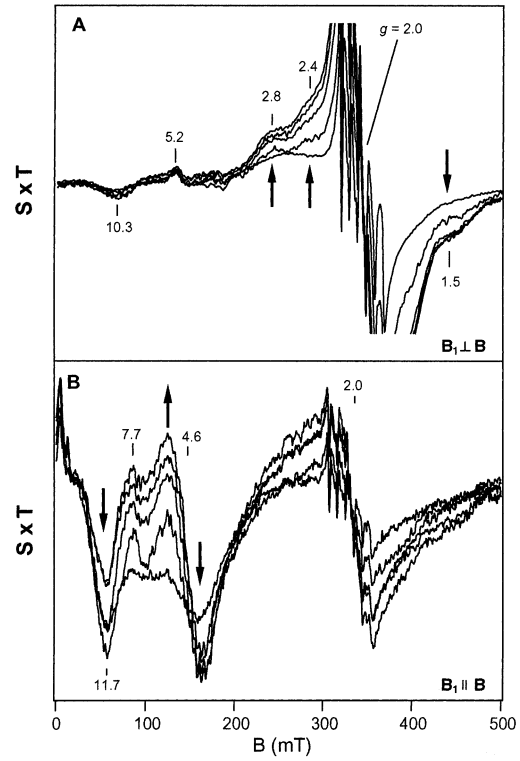

Figure 4. Perpendicular (A) and parallel mode (B) $Mn_2^{II}R2$ signals at increasing temperatures; $T = 2$, 5, 11, 18, and 23 K. The spectra are plotted as signal times temperature ($S \times T$). Instrumental conditions: microwave frequency, 9.62 GHz ($B_1 \perp B$), 9.26 GHz ($B_1 \parallel B$); microwave power, 2−63 μW ($B_1 \perp B$), 0.2−6.3 mW ($B_1 \parallel B$).

at low field due to nonlinear line shape distribution at $B = 0$.[46] Distributions in D and E/D were found to be the dominant contribution to the line shape. The observed line widths are reasonably well matched for Gaussian distributions of $\sigma_D = 0.03$ cm^{-1} and $\sigma_{E/D} = 0.05$.[47,48] The distribution in zero-field parameters renders the hyperfine patterns too broad to be observable. Thus, the signals of the mononuclear $Mn^{II}R2$ species are readily differentiated from the aquaMn^{II} species. The observed 6-line pattern is entirely from the aquaMn^{II} species. The intensities of the $Mn^{II}R2$ species and the aquaMn^{II} species both display an inverse temperature dependence, as expected for complexes with $D \ll kT$.

As the Mn^{II} is titrated above 1 equiv, the $Mn^{II}R2$ signal losses intensity and a new signals appear in both perpendicular and parallel mode. The temperature dependence of the new signals is shown in Figure 4 for a sample with 2 equiv of Mn^{II}. At the lowest temperature (2 K), the dominant signals are from small amounts of the mononuclear $Mn^{II}R2$ and aquaMn^{II} species (~0.1 eq. each). As the temperature is raised, the new signals grow in at $g = 2.8$, 2.4, 2.0 and 1.5 ($\mathbf{B_1} \perp \mathbf{B}$) and $g = 11.7$, 7.7, and 4.6 ($\mathbf{B_1} \parallel \mathbf{B}$). The spectra of Figure 4 are scaled in intensity as signal times temperature. In these plots, the intensity of species with an inverse temperature dependence (Curie Law) remains constant, while signals from excited state spin manifolds will increase in intensity with increasing temperature. The observed growth of signals with increasing temperature is indicative of

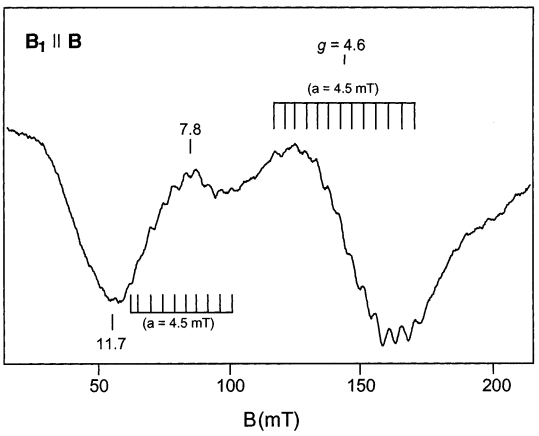

Figure 5. Expanded parallel mode $Mn_2^{II}R2$ showing a multiline hyperfine pattern with splitting of 4.5 ± 0.5 mT. Temperature, 11 K.

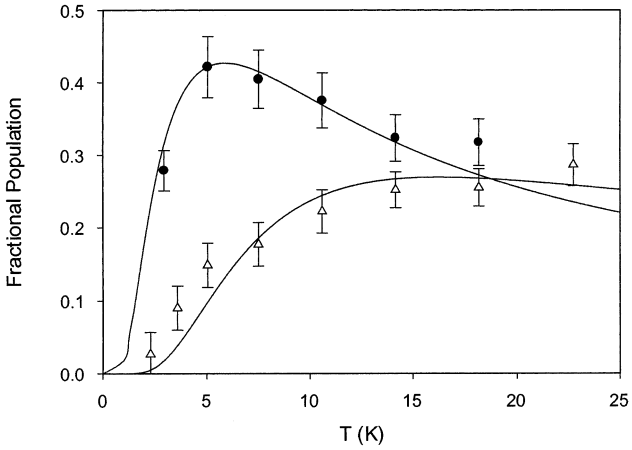

Figure 6. Signal times temperature versus temperature dependence of the $g = 11.7$ (●) and $g = 4.6$ (△) signals. The theoretical curves are the fractional populations of the $S = 1$ and $S = 2$ manifolds for $J = -1.8 \pm 0.3$ cm^{-1} from eq 2.

an antiferromagnetically coupled Mn_2^{II} site. In addition, the signals at $g = 7.7$ and 4.6 ($\mathbf{B_1} \parallel \mathbf{B}$) shown in Figure 5 in expanded scale, exhibit a multiline hyperfine pattern with an average splitting of 4.5 mT. The intensity of the signals from the $Mn_2^{II}R2$ species is 90% of maximum after addition of 2 equiv of manganese per R2, and reaches maximum at 2.3 equiv. Additional Mn^{II} above 2.3 eq. results in an increase in the aquaMn^{II} signal only, with no further changes to either $Mn^{II}R2$ or $Mn_2^{II}R2$ signals. The growth of $Mn_2^{II}R2$ species is concomitant with the loss of the $Mn^{II}R2$ species, indicating that the second Mn^{II} ion is occupying a protein site adjacent to the site of the $Mn^{II}R2$ species. Thus, there are only two distinct Mn protein binding sites for Mn, and we associate these with the normal Fe binding sites of R2.

Figure 6 shows the temperature dependence of the $g = 11.7$ and 4.6 ($\mathbf{B_1} \parallel \mathbf{B}$) resonances plotted as signal intensity times temperature versus temperature. The two signals have different temperature dependences indicating that they originate from different spin manifolds of the antiferromagnetically coupled $Mn_2^{II}R2$ site. The decrease in the signal intensity of the $g = 11.7$ resonance prior to the $g = 4.6$ signal indicates that the $g = 11.7$ signal originates from a lower lying manifold. The isotropic exchange coupling term (J) from the Heisenberg Exchange Hamiltonian ($H = -2JS_1 \cdot S_2$) can be determined from Figure 6. The data are fitted to theoretical curves using the

(46) Hendrich, M. P.; Debrunner, P. G. *Foundations of Modern EPR*; Eaton, G. R., Eaton, S. S., Salikhov, K. M., Ed; World Scientific: New Jersey, 1997; pp 530−547.
(47) Hendrich, M. P.; Debrunner, P. G. *Biopys. J.* **1989**, *56*, 489−506.
(48) Gaffney, B. J.; Mavrophilipos, D. C.; Doctor, K. S. *Biophys. J.* **1993**, *64*, 773−783.

Table 1. Distribution of Manganese[a] within R2 Homodimer at Representative Points along the Titration Curve

Mn^{II} added	$Mn^{II}R2$	$Mn_2^{II}R2$	aquaMn^{II}	% mass balance[b]
0.5	0.48	0.00	0.01	98
1.2	0.64	0.26	0.02	98
1.4	0.48	0.48	0.03	105
2.0	0.19	0.85	0.13	101
3.0	0.00	1.00	0.96	99
4.7	0.00	1.00	2.52	96

[a] Equivalents of each species per apoR2 ($\beta\beta$). [b] Percent mass balance is defined as the amount of Mn^{II} from each species divided by the amount of Mn^{II} added.

following equation for the fractional population of a spin manifold (n_S)

$$\text{intensity} \times T \approx n_S = \frac{(2S+1)e^{-JS(S+1)/kT}}{\sum_{S'}(2S'+1)e^{-JS'(S'+1)/kT}} \qquad (2)$$

As shown in Figure 6, for $J = -1.8 \pm 0.3\ cm^{-1}$, the temperature dependencies of the $g = 11.7$ and 4.6 signals can be simultaneously fit to transitions within the $S = 1$ and 2 manifolds, respectively. The $g = 2.8$ and 1.5 ($\mathbf{B_1} \perp \mathbf{B}$) resonances have the same temperature dependence as the $g = 4.6$ ($\mathbf{B_1} \parallel \mathbf{B}$) resonance, indicating that these signals are also derived from the $S = 2$ manifold.

The concentration of aquaMn^{II} was determined by double integration of the signal at $g = 2.0$ and by measurement of the 6-line hyperfine intensity. The monomeric $Mn^{II}R2$ concentration was determined by calibration of its signal intensity at low concentrations of Mn^{II} (<0.5 equiv), where the added Mn^{II} titrates linearly with the signals from the $Mn^{II}R2$ species. In addition, the simulations of Figure 3 confirmed the expected amount of $Mn^{II}R2$ species. The amount of $Mn_2^{II}R2$ formed during the titration was measured from the intensity of the $g = 4.6$ ($\mathbf{B_1} \parallel \mathbf{B}$) signal at a temperature of 15 K. At 2 equiv of Mn^{II}, the amount of $Mn_2^{II}R2$ was determined by subtracting the amount of $Mn^{II}R2$ and aquaMn^{II} species observed from the total Mn^{II} added. This value was used to establish a response factor for the $g = 4.6$ signal at this temperature. The concentration of $Mn_2^{II}R2$ at other titration points is then determined by multiplying the measured signal intensity by the response factor. At all titration points, the concentrations of $Mn_2^{II}R2$ obtained from this procedure were within 4% of the value predicted from subtracting the $Mn^{II}R2$ and aquaMn^{II} species from the total Mn^{II} added. These data indicate that the three Mn^{II} species account for all the Mn added to the sample, and there are no Mn species which are otherwise not observable by EPR. All three Mn^{II}-containing species can be accurately measured over the course of the titration. Table 1 gives representative concentrations from the full titration series. The concentrations of each of these three species per [R2] versus [Mn^{II}] added per [R2] are plotted in Figure 7. For all points on the titration curve ($n = 12$), the sum of all three species observed by EPR quantitatively agrees with the total Mn added to the sample. The titration was continued to 9 equiv (data not shown) which showed only a linear increase in the aquaMn^{II} species.

The addition of 100 mM KCl to the protein buffer was necessary for observation of bound Mn^{II} within the active site of R2. Figure S1 (see the Supporting Information) shows representative EPR signals with the addition of 3 equiv of Mn^{II} to apoR2 in the presence and absence of KCl. In the absence of KCl all Mn^{II} was quantitatively accounted for as aquaMn^{II}. In the presence of KCl, the characteristic signals from $Mn_2^{II}R2$ are observed at $g = 4.6$ and 11.7 (with correct temperature dependence), and the aquaMn^{II} signal is significantly weaker. Concentration determinations of these species from the signals found 1 equiv of $Mn_2^{II}R2$ and 1 eq of aquaMn^{II}.

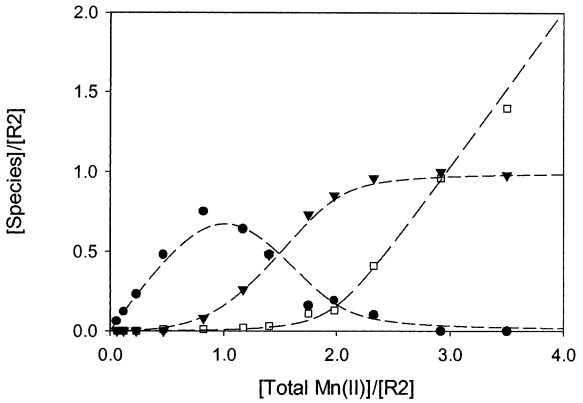

Figure 7. Equivalents of observed paramagnetic species as a function of added Mn^{II}, and theoretical curves for a two site sequential binding model with $K_1 = (5.5 \pm 1.1) \times 10^5\ M^{-1}$ and $K_2 = (3.9 \pm 0.6) \times 10^4\ M^{-1}$. The species are $Mn^{II}R2$ (●), $Mn_2^{II}R2$ (▼), and aquaMn^{II} (□).

Modeling the Binding of Manganese to apoR2. The concentration of each observable paramagnetic species ($Mn^{II}R2$, $Mn_2^{II}R2$, and aquaMn^{II}) can be fit to a sequential two site binding model described by the following equations

$$\text{apoR2} + Mn^{II} \rightleftharpoons Mn^{II}R2;\ K_1 \qquad (3)$$

$$Mn^{II}R2 + Mn^{II} \rightleftharpoons Mn^{II}R2;\ K_2 \qquad (4)$$

$$K_1 = \frac{[Mn^{II}R2]}{[\text{apoR2}][Mn^{II}]} \qquad (5)$$

$$K_2 = \frac{[Mn_2{}^{II}R2]}{[Mn^{II}R2][Mn^{II}]} \qquad (6)$$

$$[R2]_{total} = [apoR2] + [Mn^{II}R2] + [Mn_2{}^{II}R2] \qquad (7)$$

$$[Mn^{II}]_{total} = [Mn^{II}]_{aqua} + [Mn^{II}R2] + 2 \cdot [Mn_2{}^{II}R2] \qquad (8)$$

Expression of [$Mn^{II}R2$] in terms of K_1, K_2, $[R2]_{total}$, and $[Mn^{II}]_{total}$ gives a cubic equation that can be solved numerically (see the Supporting Information). Because both $[R2]_{total}$ and $[Mn^{II}]_{total}$ are known, the theoretical curves for [$Mn^{II}R2$], [$Mn_2^{II}R2$], and $[Mn^{II}]_{aqua}$ can be calculated and are dependent only on K_1 and K_2. Figure 7 shows the best fit of experimental data to the theoretical curves obtained by adjusting only K_1 and K_2 as free parameters for the observable paramagnetic species normalized to $[R2]_{total}$. No other parameters are adjustable, varying K_1 and K_2 in the calculations determines both the abscissa and ordinate scales of all three curves. The association constants determined from the fit are $K_1 = (5.5 \pm 1.1) \times 10^5\ M^{-1}$ and $K_2 = (3.9 \pm 0.6) \times 10^4\ M^{-1}$. ($K_D$ of $1.8 \pm 0.3\ \mu M$ and $25.6 \pm 3.4\ \mu M$, respectively). The mononuclear $Mn^{II}R2$ signal intensity quantitatively accounts for only one Mn^{II} per

protein, and after formation of the $Mn_2^{II}R2$ site, it is not observed again. Therefore, upon titration of up to 9 equiv of Mn^{II}, only one β-peptide of the R2 homodimer ($\beta\beta$) is completely occupied by Mn^{II}. Thus producing a Mn_2^{II} cluster in a single β-peptide and leaving the adjacent β-peptide unoccupied. This indicates that the two β-peptides of R2 do not behave identically during metal incorporation. Therefore, as mentioned in the Introduction, we introduce nomenclature to differentiate the β-peptide forming the first bimetallic cluster as β_I, and the adjacent second β-peptide as β_{II}. This distinction comes about only after binding the first equivalent of metal. Hence, addition of up to 9 equiv of Mn^{II} to apoR2 resulted in an Mn_2^{II} occupied β_I-peptide and a vacant β_{II}-peptide, i.e., $(Mn_2^{II}\beta_I)(\beta_{II})$.

Titration of apoR2 with Manganese (20% Glycerol). Previously published results from other laboratories[32,34] have demonstrated greater than 2 equiv of Mn^{II} or Fe^{II} can bind within apoR2 upon simple titration. These previous reports of metal titration into apoR2 used buffers with significantly higher concentrations of glycerol. Thus, we have considered the possibility that the buffer conditions could influence incorporation of metal into apoR2. We performed a limited titration of Mn^{II} under the conditions published by Atta et al., (100 mM Tris, pH 7.5, 20% glycerol).[34] Under these conditions, as shown in Figure S2 (Supporting Information), we observe that the $Mn^{II}R2$ species is initially formed upon addition of the up to 2 equiv Mn^{II}, after which this species decreases concomitantly with the formation of the $Mn_2^{II}R2$ species. Addition of 3.8 equiv of Mn^{II} to apoR2 generates 1.7 equiv of $Mn_2^{II}R2$ (3.4 Mn^{II} per R2). Thus, in agreement with previous reports, both β-peptides of R2 appear to be accessible to metal binding under these conditions. With the exception of glycerol content, all other buffer conditions of our previous titration are similar to typical published conditions.[15,22,23,28,32]

Following the same methodology as above for determination of the association constants, we observe for 20% glycerol both K_1 and K_2 decrease to approximately $1.0 \times 10^5\ M^{-1}$ and $1.4 \times 10^4\ M^{-1}$, respectively. The observed EPR signals of both the protein bound $Mn^{II}R2$ and $Mn_2^{II}R2$ species were identical to what was observed during our previous titration. Thus, this different buffer condition does not change the ligand coordination to the metal centers in R2. In a separate experiment, we have also added 4 equiv of Mn^{II} to a sample of apoR2 using our normal HEPES buffer conditions, except with no glycerol. For this sample, we observed only 2 equiv of Mn^{II} bound to the protein as the $Mn_2^{II}R2$ species.

Manganese Binding to $Fe_2^{II}R2$ as a function of O_2 Turnover. Using the common procedures for iron incorporation, our preparations of apoR2 bind 3.5 Fe atoms per $\beta\beta$. Iron occupancy < 4 per R2 is typical for this protein.[15,22,23,28,32] Our data demonstrates that only one Mn_2^{II} site is formed within homodimeric R2 $(Mn_2^{II}\beta_I)(\beta_{II})$ by simple titration of Mn^{II}. Although the differential binding affinity observed here for Mn^{II} agrees with previous findings for Fe^{II} titration, the reason only one β-peptide incorporates Mn^{II} was unclear. We hypothesized that perhaps the state of the β_I-peptide metals affects metal binding in the β_{II}-peptide sites. Assuming for the moment that Fe^{II} (like Mn^{II}) binds to a single β-peptide of R2 only, then apoR2 pre-loaded with 2 equiv of Fe^{II} should result in $(Fe_2^{II}\beta_I)(\beta_{II})$. This can then react with O_2 to access different oxidation states of the metal in the β_I sites. To test this hypothesis, Mn^{II} was added to samples of apoR2 pre-loaded with 2 equiv of Fe^{II}, before (Protocol 1) and after (Protocol 2) turnover with O_2. These samples were also reacted with O_2 in the presence of Mn^{II} (Protocol 3). The results for the three experimental protocols for metal incorporation, **P1**, **P2**, and **P3** are provided in Table 2.

Table 2. Equivalents[a] of Observed Species during Manganese Binding Protocols

sample condition	aquaMn^{II}	$Mn_2^{II}R2$	Y122•	$Fe^{III}Mn^{III}R2$	% Mn observed[d]
Mn^{II} present before and during O_2 exposure (**P1** & **P3**)					
before O_2	2.7	0.0	0.0	0.0	100
after O_2	1.0	0.6	0.6	0.0	81
d.t. + m.v.[b]	1.4	0.6	-	0.0	96
after O_2 [c]	1.4	0.6	-	0.2	104
Mn^{II} added after O_2 exposure (**P2**)					
after O_2	0.4	0.0	0.6	0.0	80
d.t. + m.v.[b]	0.4	0.0	-	0.0	80
after O_2[c]	0.4	0.0	-	0.1	100

[a] Equivalents of each species per R2 homodimer. [b] d.t. + m.v.; anaerobic sample reduced by dithionite and methyl viologen addition. [c] Air-oxidation of d.t. + m.v. sample. [d] Mn accounted for within the observed species divided by the total amount added.

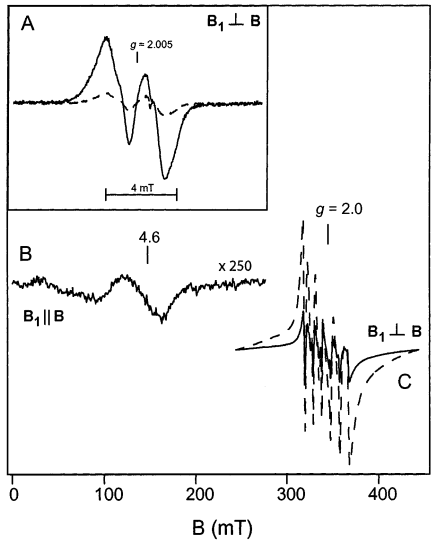

Figure 8. Perpendicular and parallel mode X-band EPR signals observed before (dashed lines) and after (solid lines) exposure to O_2. (A) Inset showing the Y122• signal. (B) Difference spectrum showing the $g = 4.6$ signal ($B_1 \| B$) from the $Mn_2^{II}R2$ species produced upon O_2 exposure. (C) Signal from aquaMn^{II}. For clarity, the Y122• signal was subtracted out of (C). Instrumental conditions: temperature, 87 K (A), 11 K (B), and 2 K (C); frequency, 9.62 GHz ($B_1 \perp B$) (A and C) 9.26 GHz ($B_1 \| B$) (B); modulation amplitude, 0.3 mT (A) and 1.0 mT (B and C); microwave power, 0.2 μW (A and C) and 2.0 mW (B).

Protocol 1: Mn^{II} Addition before O_2 Turnover (P1). To a sample of apoR2, 2 equiv of Fe^{II} were added under rigorous anaerobic conditions and allowed to incubate for 5 min. To this $(Fe_2^{II}\beta_I)(\beta_{II})$ sample, 2.7 equiv of Mn^{II} were added anaerobically. The sample was mixed by gentle agitation over the course of 5 min then the sample was frozen in liquid N_2. Figure 8C shows an EPR spectrum of this sample (dashed line). The only Mn^{II} species present is the common 6-line hyperfine signal indicative of aquaMn^{II}, whereas both $Mn^{II}R2$ and $Mn_2^{II}R2$ signals were absent. Quantitation of this signal gave 2.7 equiv of Mn^{II}, which equals the amount added. Therefore, in the absence of oxygen, Mn^{II} does not bind to $(Fe_2^{II}\beta_I)(\beta_{II})$. Furthermore, only 2 equiv of Fe^{II} are necessary to completely block Mn^{II} binding. The

lack of any bound Mn^{II} species indicates that the 2 equiv of Fe^{II} added are not occupying both β-peptides of R2 equally. If this were the case, an $Fe^{II}Mn^{II}R2$ species[32] would be produced resulting in a significant decrease in the aquaMn^{II} signal, but this decrease is not observed. Thus, in agreement with the Mn^{II} titration, 2 equiv of Fe^{II} result in occupation of only one β-peptide to give $(Fe_2^{II}\beta_I)(\beta_{II})$. Furthermore, because all of the added Mn^{II} could be observed as aquaMn^{II}, no detectable amount of Fe^{II} was displaced by Mn^{II} addition.

Protocol 2: Mn^{II} Added after O_2 Turnover (P2). To determine if the $R2_{act}$ state is responsible for Mn^{II} binding, a sample of $(Fe_2^{II}\beta_I)(\beta_{II})$ was prepared anaerobically and subsequently allowed to turnover with O_2 in the absence of Mn^{II}. Addition of 2 equiv of Fe^{II} to apoR2 produced 0.6 equiv of Y122•, as observed by EPR, upon air oxidation of $(Fe_2^{II}\beta_I)(\beta_{II})$. This represents half of the Y122• typically observed from holo$R2_{act}$ and is consistent with the commonly observed 3 Fe^{II} to 1 Y122• ratio.[15,22,23,28,32] To this oxidized sample, 0.5 equiv of Mn^{II} was added to the aerobic protein solution. The EPR spectrum of this sample showed an aquaMn^{II} signal at $g = 2$ which quantified to 0.4 equiv of Mn^{II}. No $Mn^{II}R2$ or $Mn_2^{II}R2$ signals were observed. A fraction of the added Mn (0.1 equiv) is not observed as aquaMn^{II}. Later, we will show that this can be attributed to a minority mixed metal species.

Protocol 3: Mn^{II} Present during O_2 Turnover (P3). Figure 8 illustrates the change in the EPR signals of the sample in **P1** following exposure to air by aerobic thawing and gently mixing for approximately 5 min prior to refreezing. Upon oxidation of $(Fe_2^{II}\beta_I)(\beta_{II})$ in the presence of 2.7 equiv Mn^{II}, 1.7 equiv of aquaMn^{II} was lost as indicated by reduction of the 6-line signal at $g = 2$, Figure 8C (solid line). The dashed line in Figure 8C is prior to O_2 addition. Furthermore, two additional species are now observed: the characteristic Y122• signal of $R2_{act}$ at $g = 2.005$, and signals characteristic of the $Mn_2^{II}R2$ species. The inset of Figure 8 shows EPR spectra before (dashed line) and after (solid line) exposure to O_2. Prior to air exposure, only trace levels of Y122• were observed (<0.1 equiv). However, following air exposure, the characteristic Y122• signal of $R2_{act}$ is observed. Double integration of the Y122• signal after O_2 exposure gives 0.6 equiv per R2 $\beta\beta$. In addition to the Y122• signal observed in perpendicular mode, another signal is observed in parallel mode upon O_2 exposure. Figure 8B shows the difference in the parallel mode EPR spectrum after oxidation, which shows a $g = 4.6$ signal similar to the $(Mn_2^{II}\beta_I)(\beta_{II})$ species of Figure 4B. The Mn_2^{II}-signal observed in Figure 8B has the same g-value and temperature dependence as the species in Figure 4B, indicating that an antiferromagnetically coupled $Mn_2^{II}R2$ species is formed upon turnover of $(Fe_2^{II}\beta_I)(\beta_{II})$ with O_2 in the presence of Mn^{II}. Using the known concentrations of $(Mn_2^{II}\beta_I)(\beta_{II})$ from the titration samples allows an estimate of the concentration of the $Mn_2^{II}R2$ species formed in the $(Fe_2^{II}\beta_I)(\beta_{II}) + Mn^{II} + O_2$ sample, from which we find 0.6 equiv of $Mn_2^{II}\beta_{II}$. Thus, upon turnover of the $(Fe_2^{II}\beta_I)(\beta_{II})$ site with O_2, Mn^{II} is loaded into the β_{II}-peptide to produce the differential β-peptide occupation $(Fe_2^{III}\beta_I)(Mn_2^{II}\beta_{II})$ for the majority of the protein.

The amount of $Mn_2^{II}\beta_{II}$ observed accounts for only 1.2 equiv of the total Mn^{II} lost (1.7 equiv) upon air oxidation of $(Fe_2^{II}\beta_I)(\beta_{II})$. However, in this experiment, we have not added reductant such as ascorbate or dithionite to supply the fourth electron necessary in the catalytic cycle of R2 during Y122• generation. This fourth electron could come from either Fe^{II} [21] or Mn^{II} in this sample. EPR detection of Mn^{III} ($S = 2$) is less sensitive and more complicated than Mn^{II} because it is a non-Kramer's ion. Typically, Mn^{III} species exhibit a 6-line hyperfine signal near $g = 8$ split by ~10 mT in parallel mode EPR.[49] The signal intensity would be fairly low and may be overwhelmed by the half-field transitions of aquaMn^{II}, which also have signals in this region. Therefore, a slight excess of the reductant dithionite with catalytic amounts of methyl viologen was added to the sample to reduce any Mn^{III} produced. Upon reduction of the sample, the 6-line signal at $g = 2$ associated with aquaMn^{II} increased in intensity to account for an additional 0.4 equiv of aquaMn^{II} lost upon air oxidation of $(Fe_2^{II}\beta_I)(\beta_{II})$ in the presence of Mn^{II}. This indicates that the fourth electron necessary for Y122• formation by $(Fe_2^{II}\beta_I)(\beta_{II})$ oxidation was, in part, provided by Mn^{II} during turnover with O_2. The amount of Mn^{II} recovered after reduction plus the amount of $Mn_2^{II}R2$ produced accounts for 1.6 equiv of the Mn^{II} lost (1.7 equiv) after oxidation, as given in Table 2. Typically, Mn^{III} ions disproportionate to Mn^{II} and Mn^{IV} in aqueous solutions.[50] However, we suspect that the Mn^{III} produced is adventitiously bound to the protein. Mn^{III} is expected to have low rates of ligand exchange, and thus disproportionation of Mn^{III} due to a bimolecular reaction would be inhibited.

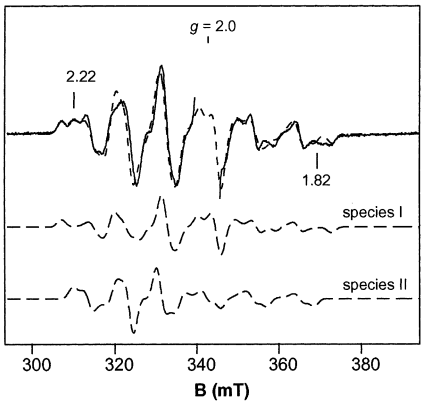

Figure 9. Perpendicular mode X-band EPR spectra (solid line) and simulations (dashed lines) of the mixed metal $Fe^{III}Mn^{III}R2$ signal. For clarity, the Y122• signal was cut out. The least-squares fit on the data is the sum of two species (0.62 species **I** + 0.38 species **II**). Instrumental conditions: temperature, 11 K; frequency, 9.62 GHz; ($B_1 \perp B$); modulation amplitude, 0.1 mT; microwave power, 0.2 mW. Simulation parameters for species **I** and **II** are given in Table 3.

Detection of a Mixed Metal $Fe^{III}Mn^{III}R2$ Species. In samples of $(Fe_2^{II}\beta_I)(\beta_{II})$ where Mn^{II} was present during O_2 turnover (**P3**) and where Mn^{II} was added after turnover (**P2**), a minor fraction of the added manganese (0.3 equiv **P3**, 0.1 equiv **P2**) was not observed as aquaMn^{II}, $Mn^{II}R2$, or $Mn_2^{II}R2$. However, reductive cycling of these samples in the presence of O_2 with excess dithionite (5×) and catalytic amounts of methyl viologen resulted in the generation of a new signal shown in Figure 9. This new signal has a 6-line hyperfine pattern centered at $g = 2.0$ ($\mathbf{B_1} \perp \mathbf{B}$).

The observed hyperfine splitting of this signal ($a = 11$ mT) is significantly larger than expected for Mn^{II} signals ($a = 9.5$

(49) Campbell, K. A.; Yikilmaz, E.; Grant, C. V.; Gregor, W.; Miller, A.-F.; Brit, D., R. *J. Am. Chem. Soc.* **1999**, *121*, 4714−4715.
(50) Cotton, A. F.; Wilkinson, G. *Advanced Inorgainic Chemistry*, 4th ed.; John Wiley & Sons: New York, 1980; p 741.

Table 3. Spectral Parameters Used for Simulation of the $Fe^{III}Mn^{III}$R2 Signal

species	*g*-values[b] (g_x, g_y, g_z)	*A*-values[b] (A_x, A_y, A_z) MHz	fraction of signal (%)
I	(2.0396, 2.0200, 2.0134)	(250, 371, 267)	62
II	(2.0527, 2.0132, 2.0357)	(184, 309, 314)	38
$Fe^{III}Mn^{III}$TACN[a]	2.037	314	

[a] $Fe^{III}Mn^{III}(\mu\text{-O})(\mu\text{-MeCO}_2)_2$ TACN complex from refs 52 and 53, isotropic values only. [b] *g* and *A*-values for the coupled basis set.

mT).[51] This signal is observed at $g = 2$, suggesting it originates from an $S = 1/2$ doublet. Possible species containing Mn exhibiting a $S = 1/2$ state low in energy are the antiferromagnetically coupled dinuclear clusters of $Mn^{II}Mn^{III}$, $Mn^{III}Mn^{IV}$, $Fe^{II}Mn^{II}$ or $Fe^{III}Mn^{III}$.[32,52−56] However, if an exchange-coupled pair of manganese ions were participating in this signal a hyperfine pattern with more than 6 lines would be expected, ruling out the first two clusters. EPR signals with similar hyperfine splittings have been observed previously for a mixed metal $Fe^{III}Mn^{III}$ model complex.[52,53] This assignment is confirmed by simulations of the observed signal shown in Figure 9. The simulations are for two $S = 1/2$ species with *g* and *A*-values given in the Table 3. The anisotropy in *g* and *A* is consistent with that observed for Mn^{III} species.[56] The signal has considerably higher resolution than the powder spectrum published for the model complex.[52,53] Although the features of the signal shown here all fall within the broader resonance of the model system, the triplet type splitting marked at $g = 2.22$ and 1.86 cannot be fit by a single species.[57] However, the simulation is significantly improved with the inclusion of a second species. The simulation shown is the addition of two $S = 1/2$ species (**I** and **II**) in relative amounts of 62% and 38%. The spectral parameters for species **I**, **II**, and the $Fe^{III}Mn^{III}$ model complex are given in Table 3.

The magnitude of the exchange coupling can be determined from the temperature dependence. The temperature dependence of the $g = 2.0$ resonance, plotted as signal intensity times temperature versus temperature, is shown in Figure 10. The signal decreases as temperature is increased indicating depopulation of the $S = 1/2$ manifold. Therefore, this signal must originate from the doublet lowest in energy. The best fit to the data is shown, giving $J = -18 \pm 3$ cm^{-1}, ($H = -2JS_1 \cdot S_2$).

It is possible that the $g = 2$ signal could also originate from an $Fe^{III}Mn^{III}$ cluster adventitiously bound to the outside of the protein. To test for this, a 20-fold excess of dithionite (without mediator) was added to a sample containing this species. Upon addition of dithionite, no effect was observed on the signal intensity until a catalytic amount of methyl viologen was added,

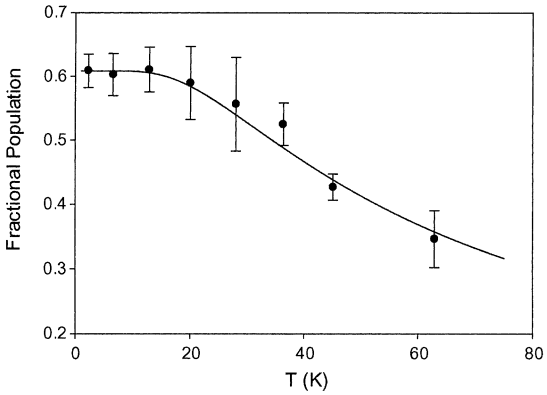

Figure 10. Signal times temperature versus temperature dependence of the $g = 2$ signal from the $Fe^{III}Mn^{III}$R2 species shown in Figure 9. The theoretical curve is the fractional population of the S = 1/2 ground state with $J = -18 \pm 3$ cm^{-1}, ($H = -2JS_1 \cdot S_2$).

at which point the signal vanished. Because the mediator methyl viologen is necessary to reductively quench the signal, the mixed metal $Fe^{III}Mn^{III}$ cluster must reside within R2, rather than adventitiously bound to the protein.

For samples of $(Fe_2^{II}\beta_I)(\beta_{II})$ with Mn^{II} added during and after O_2 turnover, the $Fe^{III}Mn^{III}$R2 signal represents 0.3 and 0.1 equiv per $\beta\beta$, respectively. Table 2 summarizes the distribution of manganese species created upon initial exposure of $(Fe_2^{II}\beta_I)(\beta_{II})$ with Mn^{II} added during (**P3**) and after O_2 turnover (**P2**). The formation of this $Fe^{III}Mn^{III}$R2 species likely originates from the oxidation of an $Fe^{II}Mn^{II}$R2 species present during turnover with O_2. The reduced mixed metal cluster could be formed either by competition for binding sites under anaerobic conditions or by metal mixing during turnover with O_2. However, because all of the Mn^{II} added to $(Fe_2^{II}\beta_I)(\beta_{II})$ was observed as aquaMn^{II}, no significant amount of $Fe^{II}Mn^{II}$R2 species could have been present prior to turnover. Therefore, the $Fe^{II}Mn^{II}$R2 species is more likely produced during reductive cycling with mediator, reductant, and O_2.

Discussion

Mechanism of apoR2 Metal Incorporation. The titration of apoR2 presented here unequivocally demonstrates that once one β-peptide of R2 (β_I) binds the first Mn^{II} ion, the adjacent binding site on β_I is occupied next, producing a dinuclear Mn_2^{II} cluster and an unoccupied second β-peptide (β_{II}) to give $(Mn_2^{II}\beta_I)(\beta_{II})$. After formation of this cluster, no further mono or dinuclear Mn^{II} species are formed with up to 9 equiv of Mn^{II} added. To our knowledge, this is the first indication that the two β-peptides of R2 do not act independently of each other. We also show that these results extend to the physiological relevant metal, iron. The anaerobic addition of 2 equiv of Fe^{II} to apoR2, followed by 2.7 equiv of Mn^{II} exhibited no bound Mn^{II} species. Because all of the added Mn^{II} is observed as aquaMn^{II}, no mixed metal $Fe^{II}Mn^{II}$R2 species was formed. This species has been observed previously,[32] therefore, there is no reason to suggest that Fe^{II} binding to apoR2 prevents Mn^{II} from binding within the same β-peptide. This suggests that both equivalents of Fe^{II} are bound within a single β-peptide to give $(Fe_2^{II}\beta_I)(\beta_{II})$ and that Mn^{II} binding within the opposite β-peptide is prevented.

On the basis of these results and a body of previous work to be discussed next, we suggest Scheme 1 for metal uptake in the absence of R2 activation.

(51) Reed, G. H.; Markham, G. D. *Biological Magnetic Resonance*; Berliner, L. J., Reuben, J., Eds.; Plenum Press: New York, 1984; *Vol 6*, pp 73−142.
(52) Bossek, U.; Weyhermüller, T.; Wieghardt, K.; Bonvoisin, J.; Girerd, J. J. *J. Chem. Soc. Chem. Commun.* **1989**, 633−636.
(53) Que, L., Jr.; True, A. E. *Progress in Inorganic Chemistry, Bioinorganic Chemistry*; Lippard, S. J., Ed.; John Wiley & Sons: New York, 1990; Vol. 38, pp 97−200.
(54) Gelasco, A.; Bensick, S.; Pecararo, V. L. *Inorg. Chem.* **1998**, *37*, 3301−3309.
(55) Holman, T. R.; Wang, Z.; Hendrich, M. P.; Que, L., Jr. *Inorg. Chem*. **1995**, *34*, 134−139.
(56) Zheng, M.; Khangulov, S. V.; Dismukes, G. C.; Barynin, V. V. *Inorg. Chem.* **1994**, *33*, 382−387.
(57) We have also considered the possibility of noncoaxial *g* and *A*-tensors. However, allowing for noncoaxial coordinate systems did not improve the accuracy of the fit or account for the observed triplet splittings observed at $g = 2.22$ and 1.86.

Scheme 1

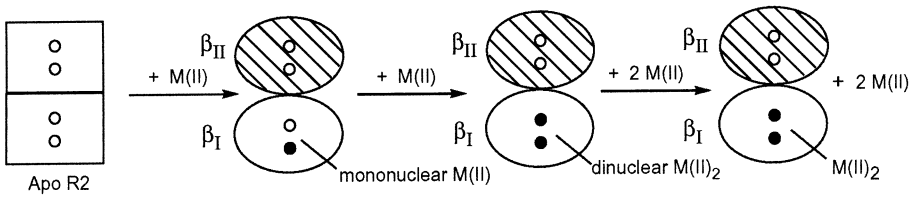

The first metal equivalent binds to only one β-peptide to give (Mβ_I)(β_{II}). This first metal alters the conformation of the whole protein homodimer to restrict metal binding at the second β-peptide (β_{II}). This conformational change occurs after binding of the first metal, since the mononuclear Mn^{II}R2 species does not exceed 1 equiv. The second equivalent of metal does not bind to β_{II} as expected, rather the metal binds adjacent to the first metal on β_I, resulting in ($M_2\beta_I$)(β_{II}). No further metal uptake is observed beyond the addition of 2 equiv.

Stubbe and co-workers first suggested the concept of a protein conformational change as an explanation for a kinetic lag phase observed during the formation of active R2 upon mixing apoR2, Fe^{II}, and O_2. Moreover, our observation that metal binding within β_{II} is dependent on O_2 activation on the β_I cluster, indicates that the two β-peptides do indeed exhibit some type of allosteric interaction.

The Mössbauer spectroscopy data of Huynh et al. indicated that the Fe_B site has a 5-fold higher binding affinity than the Fe_A site.[33] Our results with Mn^{II} also indicate a significant difference in binding affinity between the two sites (K_1/K_2 = 14). However, we suggest that the binding affinities measured for Fe_B and Fe_A sites in this previous work are for β_I only and not for both monomers, β_I and β_{II}. Because crystal structures of Mn_2^{II}R2[34] show the same protein ligation as reduced Fe_2^{II}R2,[17,18] binding of Mn^{II} by R2 should be similar to that observed for Fe^{II}.[32,33] Furthermore, the MCD spectroscopic data of Solomon et al. indicates that as with Fe^{II}, Mn^{II} preferentially binds within the B-site.[32] Therefore, the Mn^{II} species observed during titration are assigned as ($Mn^{II}\beta_I$)(β_{II}) and ($Mn_BMn_A\beta_I$)-(β_{II}), with association constant of K_1 and K_2, respectively, stated in the results. The Mn^{II} binding affinities determined here for R2 sites A and B are consistent with other protein bound Mn^{II} centers of similar coordination.[58,59]

The aforementioned MCD titration finds saturation of both the Fe_B and Fe_A sites of β_I and β_{II} at approximately 3 equiv of Fe^{II}.[32] Furthermore, previous EPR titrations of apoR2 with Mn^{II} performed by Fontecave et al. indicated that 4 equiv of Mn^{II} could be incorporated by apoR2.[34] Also, the crystal structure of MnR2 shows incorporation of 4 Mn ions.[34,60] We have demonstrated here that under identical conditions as reported by the Fontecave et al. (20% glycerol) apoR2 is capable of binding nearly 4 equiv of Mn^{II} per R2. However, under our buffer conditions of 5% glycerol or less, we clearly observe only 2 equiv or Mn^{II} binding per R2. We conclude that high levels of glycerol result in a loss of the allosteric effect between the β-monomers of R2. Although high levels of glycerol are not native for the protein, our experiments are in the absence of the R1 subunit of RNR. Thus, experiments in the presence of the R1 subunit are needed to determine if this newly observed allosteric effect is present. Nevertheless, the isolated R2 subunit of RNR is the subject of much previously published work, and our findings are certainly relavent for that body of work. We have shown that other buffer conditions are also important for metal binding. Lower concentrations of KCl resulted in no Mn^{II} binding internal to R2. Because R2 is an acidic protein, we suspect that the addition of cations to the buffer inhibits binding to external protein sites.

Our results for Mn incorporation indicate that only two metal ions are incorporated during a titration in buffers with less than 5% glycerol. We also believe that the conformational change proposed by Stubbe et al. occurs after binding a single metal atoms to the R2 homodimer.[29] However, these results do raise the important question as to how full metal incorporation is achieved. Interestingly, the answer involves the O_2 turnover chemistry of R2. Scheme 2 summarizes the results, which demonstrate that R2 activation chemistry is required for metal incorporation into the β_{II}-peptide. Our rational for using both Fe and Mn in these experiments was that we can easily quantify the partitioning of Mn species in R2 separately from the Fe species, into aquaMn^{II}, mononuclear Mn^{II}R2, or dinuclear Mn_2^{II}R2 species.

The discussion starts on the left side of Scheme 2 with the protein in the ($Fe_2^{II}\beta_I$)(β_{II}) state. The addition of Mn^{II} to ($Fe_2^{II}\beta_I$)-(β_{II}) (upper pathway) has no effect. Nearly all of the added Mn^{II} is observed as aquaMn^{II}. Next, the ($Fe_2^{II}\beta_I$)(β_{II}) state is exposed to O_2, (lower pathway) resulting in the formation of active β_I sites ($Fe_2^{III}\beta_I$; Y122•)(β_{II}). Addition of Mn^{II} to this active state also shows no effect. Again, nearly all of the added Mn^{II} is observed as aquaMn^{II}.

The key observation is the second step of the upper pathway. With the ($Fe_2^{II}\beta_I$)(β_{II}) site poised for turnover in the presence of Mn^{II}, upon O_2 addition we observe the formation of Mn_2^{II} clusters and Y122• in equal amounts. The amount of Y122• produced is as expected based on the accepted 3 Fe^{II} to 1 Y122• stoichiometry of R2.[13,19−22] However, it is interesting to note that the 'extra' electron necessary for generation of Y122• is supplied in part by Mn^{II}. As with previous turnover experiments, even when enough Fe^{II} and electrons are present for complete Y122• generation, only 2/3 of the Fe_2^{II}R2 sites produce radical. The outcome of the remaining Fe_2^{II}R2 remains unclear. The amount of Y122• generated and Mn_2^{II} sites formed requires that the Mn predominately binds within the vacant β_{II} peptide, because Y122• radicals are not generated by the Mn_2^{II}R2 site. It is possible that the less than full occupation of β_{II} under these conditions can in part be attributed to competition between Fe^{II} and Mn^{II} for binding sites under anaerobic conditions. Formation of inactive mixed metal FeMn clusters within β_I would detract from the amount of cycled R2, and thus Y122• generated.

(58) Rusnak, F.; Yu, L.; Todorovic, S.; Mertz, P. *Biochemistry* **1999**, *38*, 6943−6952.
(59) D'souza, V. M.; Swierczek, S. I.; Cosper, N. J.; Meng, L.; Ruebush, S.; Copik, A. J.; Scott, R. A.; Holtz, R. C. *Biochemistry* **2002**, *41*, 13 096−13 105.
(60) Hogbom, M.; Andersson, M. E.; Nordlund, P. *JBIC* **2001**, *6*, 3, 315−323.

Scheme 2

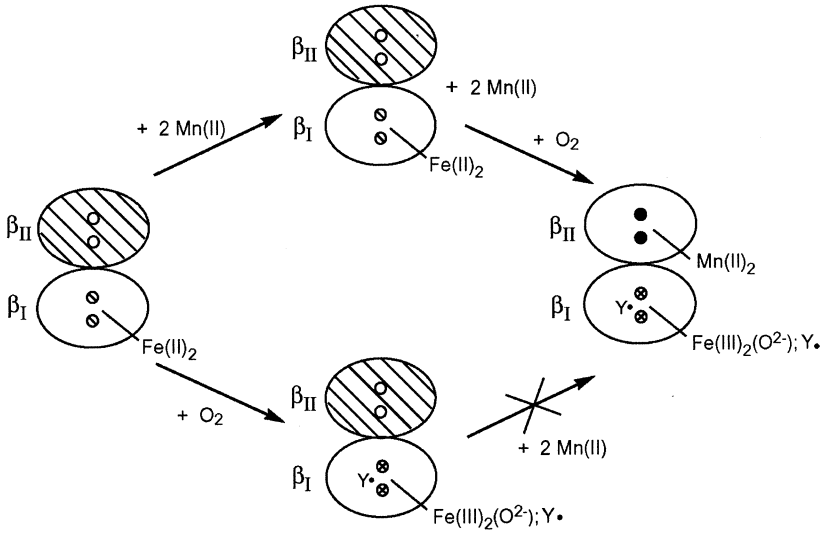

The incorporation of Mn_2^{II} into β_{II} only during O_2 turnover at amounts equal to the Y122• concentration suggests that there is a state of the protein in R2 activation chemistry which facilitates metal binding within the β_{II} peptide sites. The current models for the reductive activation of O_2 and generation of Y122• are based on the observation of an intermediate **X** in the reaction shown below.[15,13,21,28,29,61]

$$\mathrm{Fe_2^{II}; Tyr\text{-}OH} \xrightarrow[k_1 = 60\text{-}80\ s^{-1}]{O_2 + e^-} \mathrm{(H_2O)Fe^{III}(O^{2-})Fe^{IV}; Tyr\text{-}OH} \xrightarrow[k_2 = 0.7\text{-}1.0\ s^{-1}]{} \mathrm{Fe_2^{III}(O^{2-}); Tyr\text{-}O\bullet}$$

$\mathbf{R2_{red}}$ **X** $\mathbf{R2_{act}}$

Another intermediate, **U**, which contains a protonated tryptophan radical is neglected in the above reaction due to its short lifetime ($k > 20\ s^{-1}$).[15,13,62] Compound **X** is observable because its rate of consumption is significantly slower than its rate of creation.[25−27] Because **X** exists for a significant period of time, we speculate that when **X** is present, the protein is in a conformation that favors β_{II} metal binding.

In light of these results, we propose that addition of excess Fe^{II} to apoR2 produces a single O_2 reactive diferrous cluster within only one β-peptide of R2, to give $(Fe_2^{II}\beta_I)(\beta_{II})$. Then, during turnover with O_2, a second diferrous cluster is generated on the adjacent β_{II}-peptide and capable of Y122• formation, $(Fe_2^{III}(O^{2-})$; Y122•$\beta_I)(Fe_2^{II}\beta_{II})$. This model could explain why the theoretical complement of 4 Fe per R2 is not observed. As previously mentioned, the average experimentally observed ratios for Y122• production and Fe incorporation per R2 are 1.2 and 3.2−3.6, respectively.[15,22,23,28,32] If only Fe_2^{II}R2 sites, which produce Y122• are capable of full Fe incorporation, generation of 1.2 Y122• per R2 corresponds to 0.6 equiv of R2 capable of binding 4 Fe per R2. Therefore, the Y122• producing fraction corresponds to 2.4 equiv Fe per R2. The remaining 0.8 equiv of un-oxidized Y122−OH corresponds to 0.4 equiv of R2, which did not participate in the O_2 activation chemistry, and therefore can only bind 2 Fe per R2. Thus, corresponding to an additional 0.8 equiv Fe per R2. The sum of both fractions (2.4 + 0.8 equiv) yields 3.2 Fe per R2, which is consistent with experimental observations of low Fe occupancy in R2.

Electronic Characteristics of Mn species. A quantitative interpretation of EPR spectra from mononuclear Mn^{II} proteins has generally been limited to Mn^{II} sites with low anisotropy, $D < 0.03\ cm^{-1}$. For such proteins, the spectra show hyperfine lines with forbidden transitions and the analysis of this spectra is based on these forbidden transitions.[51] For Mn sites in proteins such as R2 with high anisotropy ($D = 0.1\ cm^{-1}$), the spectra are complicated and interpretation requires a different approach, which is demonstrated here. The simulations provided for the Mn^{II}R2 species are novel in that they represent the first published quantitative analysis for such proteins utilizing both perpendicular and parallel mode spectra at two different frequencies (X- and Q-band). The intensity scale of our simulations is determined by the species concentration. We find that both the X- and Q-band simulations quantitatively agree to within 12% of the Mn^{II} concentration.

The larger *D*-value is consistent with a protein site that has substantial protein ligation and low water ligation.[63] More detailed assessment would benefit from the addition of structurally characterized complexes with larger *D*-values. Given the greater binding affinity observed from the Fe_B site relative to the Fe_A site, the Mn^{II}R2 signal is assigned to Mn^{II} binding in the B site of a single β-peptide within apoR2, $(Mn_B^{II}\beta_I)(\beta_{II})$. The large rhombicity ($E/D = 0.21$) is consistent with the low symmetry exhibited in the crystal structure.[34] The line shape of the spectra is dominated by distributions in the zero-field parameters. The width of the distributions is substantial, approximately 30% of the central value, which has been observed for iron proteins.[47,48] Quantitative treatment of these signals must include proper treatment of such distributions.

The crystal structure of the Mn_2^{II}R2 protein shows two Mn ions bridged by two carboxylato ligands. In agreement, the EPR spectra of the Mn_2^{II}R2 species show similarities to previous Mn_2^{II}-complexes with carboxylato bridging ligands and similar metal−metal distances.[64] Furthermore, the measured coupling,

(61) Bollinger, J. M., Jr.; Tong, W. H.; Ravi, N.; Huynh, B. H.; Edmondson, D. E.; Stubbe, J. *J. Am. Chem. Soc.* **1994**, *116*, 8024−8032.
(62) Bollinger, J. M., Jr.; Stubbe, J.; Huynh, B. H.; Edmondson, D. E. *J. Am. Chem. Soc*. **1991**, *113*, 6289−6291.
(63) Smoukov, S. K.; Telser, J.; Bernat, B. A.; Rife, C. L.; Armstrong, R. N.; Hoffman, B. M. *J. Am. Chem. Soc.* **1916**, *38*, S **2002**, *124*, 10, 2318−2326.
(64) Golembek, A. P.; Hendrich, M. P., unpublished results.

$J = -1.8$ cm^{-1}, is comparable to values reported for such complexes.[65−67] The multiline splitting of 4.5 mT is also comparable to that observed for other spin-coupled Mn_2^{II}-centers.

In samples containing both Fe^{II} and Mn^{II} for the O_2 turnover experiments, a new paramagnetic species is observed which is unambiguously assigned to a mixed metal $Fe^{III}Mn^{III}$ cluster within the protein. This minor species likely results from competition between Fe^{II} and Mn^{II} for R2 sites, whereas in the reduced state or during reductive cycling. The reduced mixed-metal species $Fe^{II}Mn^{II}$R2 has been reported previously.[32] Although we did not see evidence by EPR that this species was formed, *g*-values for Fe^{II} can be highly anisotropic compared to Mn^{II} or Fe^{III}, which would significantly broaden the $S = 1/2$ signal of $Fe^{II}Mn^{II}$R2, and thereby make it difficult to detect under the intense aquaMn^{II} signal. Under anaerobic conditions, all Mn^{II} added to $(Fe_2^{II}\beta_I)(\beta_{II})$ is accounted for as aquaMn^{II}. Therefore, displacement of Fe^{II} for Mn^{II} in the absence of turnover does not appear to occur. Consequently, we believe that this $Fe^{II}Mn^{II}$R2 species is generated by metal mixing during reductive cycling with mediator, reductant, and O_2. The observed $Fe^{III}Mn^{III}$ species is presumably produced by the 2-electron oxidation of the $Fe^{II}Mn^{II}$R2 species during reductive cycling. The $Fe^{III}Mn^{III}$R2 species can only be reduced in the presence of a mediator like methyl viologen, the same mediator commonly used for reduction of the native iron containing protein. Therefore, the $Fe^{III}Mn^{III}$ site must reside within protein, rather than adventitiously bound. We suggest that species **I** and **II** used for simulation of the $Fe^{III}Mn^{III}$R2 signal originates from different Fe^{II} containing sites, Fe_A or Fe_B, displaced by Mn^{II}. Thus, the observed signal is a combination of $Mn_A^{III}Fe_B^{III}$ and $Fe_A^{III}Mn_B^{III}$ species within R2. The lower binding affinity observed for Fe^{II} [32] in site A makes displacement of the Fe_A more favorable than Fe_B. Therefore, species **I**, which comprises the greater fraction of the $Fe^{III}Mn^{III}$R2 signal, is believed to originate from $Mn_A^{III}Fe_B^{III}$R2. Consequently, species **II** assigned to $Fe_A^{III}Mn_B^{III}$R2.

The EPR signal of the $Fe^{III}Mn^{III}$R2 species reported here is comparable to that of $Fe^{III}Mn^{III}$TACN.[52,53] Both the hyperfine splittings and *g*-values for the $S = 1/2$ state are similar. However, the exchange coupling observed for $Fe^{III}Mn^{III}$R2 (-18 cm^{-1}) is significantly lower than $Fe^{III}Mn^{III}$TACN (-73 cm^{-1}). The crystal structure of the $Fe^{III}Mn^{III}$TACN complex shows an oxo-bridge between the two metals. The magnitude of *J* for the $Fe^{III}Mn^{III}$R2 species is too large to be attributed to carboxylato bridging alone, but low compared to the TACN complex. Thus, we suggest the presence of a substituted single atom bridging ligand such as a μ-hydroxo or μ-carboxylato group within the $Fe^{III}Mn^{III}$R2 site.

Conclusion

We provide compelling evidence of an allosteric effect between the two β-peptides during the uptake of metal into the R2 subunit of ribonucleotide reductase. We suggest that upon binding of the first metal into a single β-peptide (β_I) of apoR2, a conformational change occurs which prevents metal from binding to the β_{II} peptide. However, metal incorporation in the β_{II}-peptide occurs upon $(Fe_2^{II}\beta_I)(\beta_{II})$ catalyzed O_2 activation. This model for R2 metal incorporation can explain the generally observed low Fe occupation of R2.

We also demonstrate that metal uptake and the allosteric effect are sensitive to buffer conditions. Higher levels of glycerol result in loss of the newly observed allosteric effect. Although high levels of glycerol are not native for the protein, the effect of the R1 subunit of RNR on this allosteric effect is unknown. Nevertheless, the isolated R2 subunit of RNR is the subject of much previously published work, and our findings are certainly relavent for that body of work.

Abbreviations: RNR, ribonucleotide reductase; R2, small subunit of ribonucleotide reductase R2; $R2_{red}$, fully reduced diferrous R2; $R2_{act}$, active form of R2 [Fe_2^{III}R2; Tyr•]; $\beta\beta$, R2 homodimer; β_I, first single β-strand of R2 to bind metal; β_{II}, second single β-strand of R2 to bind metal; $Fe_2^{II}\beta_I$, apo R2 with 2 equivalents of Fe^{II} per R2 homodimer; Mn^{II}R2, mononuclear Mn^{II} substituted R2; Mn_2^{II}R2, binuclear Mn^{II} substituted R2; $Mn_2^{II}\beta_I$ and $Mn_2^{II}\beta_{II}$, binuclear Mn_2^{II} cluster on first and second β-strand, respectively; $Fe^{III}Mn^{III}$R2, mixed metal cluster within R2; MnCat, manganese catalase; TACN, *N*,*N*′,*N*″-trimethyl-1,4,7-triazacyclononane; EPR, electron paramagnetic resonance; HEPES, 4-(2-hydroxyethyl)piperazine-1-ethanesulfonic acid.

Acknowledgment. This work was supported from a grant by NIH 49970 (M.P.H). We thank Caleb Culver for help in acquiring the Q-band data and microwave cavity construction.

Supporting Information Available: Representative EPR signals with the addition of 3 equiv of Mn^{II} to apoR2 in the presence and absence of KCl, cubic equation expression of $[Mn^{II}R2]$ in terms of K_1, K_2, $[R2]_{total}$, and $[Mn^{II}]_{total}$. Perpendicular and parallel mode X-band EPR spectra for 3 equiv Mn^{II} added to apoR2 in the presence of 100 mM KCl (dashed line) and absence of any KCl (solid line) (Figure S1), and equivalents of observed paramagnetic species as a function of added Mn^{II} in 20% glycerol (Figure S2). This material is available free of charge via the Internet at http://pubs.acs.org.

JA021290H

(65) Khangulov, S. V.; Pessiki, P. J.; Barynin, V. V.; Ash, D. E.; Dismukes, G. C. *Biochemistry* **1995**, *34*, 2015−2025.
(66) Flassbeck, C.; Weighardt, K.; Bill, E.; Butzlaff, Ch.; Trautwein, A. X.; Nuber, B.; Weiss, J. *Inorg. Chem.* **1992**, *31*, 21−26.
(67) Yu, S.-B.; Lippard, S. J.; Shweky, I.; Bino, A. *Inorg. Chem.* **1992**, *31*, 3502−3504.